ACS APPLIED MATERIALS & INTERFACES

www.acsami.org

Research Article

Enhanced Adhesion Energy at Oxide/Ag Interfaces for Low-Emissivity Glasses: Theoretical Insight into Doping and Vacancy Effects

David Cornil, Nicolas Rivolta, Virginie Mercier, Hughes Wiame, David Beljonne, and Jérôme Cornil*

Cite This: *ACS Appl. Mater. Interfaces* 2020, 12, 40838–40849

Read Online

ACCESS | Metrics & More | Article Recommendations | Supporting Information

ABSTRACT: Low-emissivity glasses rely on multistacked architectures with a thin silver layer sandwiched between oxide layers. The mechanical stability of the silver/oxide interfaces is a critical parameter that must be maximized. Here, we demonstrate by means of quantum-chemical calculations that a low work of adhesion at interfaces can be significantly increased *via* doping and by introducing vacancies in the oxide layer. For the sake of illustration, we focus on the $ZrO_2(111)/Ag(111)$ interface exhibiting a poor adhesion in the pristine state and quantify the impact of introducing n-type dopants or p-type dopants in ZrO_2 and vacancies in oxygen atoms (nV_O; with n = 1, 2, 4, 8, 10, 16), zirconium atoms (mV_{Zr}; with m = 1, 2, 4, 8), or both ($nV_O + mV_{Zr}$; with m/n = 1:2, 1:4, 2:2, 2:4). In the case of doping, interfacial electron transfer promotes an increase in the work of adhesion, from initially 0.16 to ∼0.8 J m^{-2} (n-type) and ∼2.0 J m^{-2} (p-type) at 10% doping. A similar increase in the work of adhesion is obtained by introducing vacancies, *e.g.*, V_O [V_{Zr}] in the oxide layer yields a work of adhesion of ∼1.5−2.0 J m^{-2} at 10% vacancies. An increase is also observed when mixing V_O and V_{Zr} vacancies in a nonstoichiometric ratio ($nV_O + mV_{Zr}$; with $2n \neq m$), while a stoichiometric ratio of V_O and V_{Zr} has no impact on the interfacial properties.

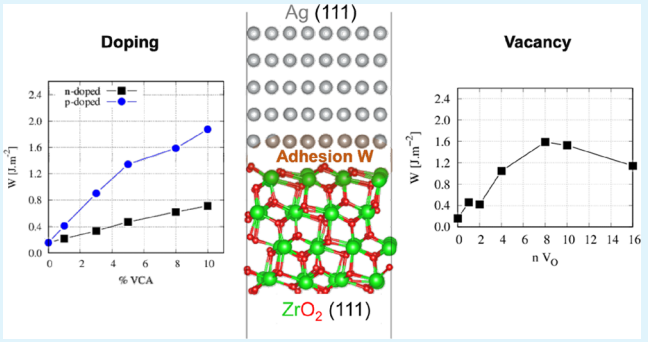

KEYWORDS: *work of adhesion, interface, DFT, doping, vacancy*

1. INTRODUCTION

Nowadays, the reduction of energetic costs is a global issue in many areas. In the field of building construction or car production, the development of low-emissivity (low-e) glasses that reflect infrared (*i.e.*, heat) and ultraviolet light is a major path to control heating and improve comfort in habitable spaces.[1,2] Low-e glasses rely on multilayered architectures incorporating silver in contact with various metal oxides (typically ZnO, TiO_2, SnO_2).[3−8] Among all of these oxides, zirconia (ZrO_2) is another material of interest that is widely used in a large range of technical and biomedical applications[9−12] due to its good mechanical properties, in particular its high strength and fracture toughness.[13,14] This has already motivated many works focusing on the adhesion of zirconia on various metals such as Ni, Cu, or Pt.[15] As a result, ZrO_2 could also prove to be a material of choice in low-emissivity glasses. However, our previous theoretical calculations indicate that the defect-free $ZrO_2(111)/Ag(111)$ interface exhibits a very poor adhesion.[16] The mechanical properties of heterogeneous materials depend mostly on the strength of adhesion between their components.[17] Therefore, one challenge in this field is to promote a strong adhesion at the metal oxide/metal interface. Optimizing the adhesion energy between the two materials is not a simple task since this property depends on many parameters. Many studies have already been made at the theoretical level to investigate the origin of interface adhesion and have demonstrated that this property is strongly connected to the formation of chemical bonds at the interface. Density functional theory (DFT) calculations made on ZnO, TiO_2, SnO_2, or ZrO_2/metal interfaces have also shown that a weak work of adhesion is typically associated with a low interfacial charge transfer and *vice versa*.[16,18−21] This connection was also observed for other kinds of interfaces such as oxide/oxide[22] or metal/carbide.[23] Therefore, a fine control of the nature of the interface chemistry appears to be mandatory to obtain a strong adhesion. The modification of the charge distribution at the interface is one key ingredient that can be manipulated to tune

Received: April 24, 2020
Accepted: August 17, 2020
Published: August 17, 2020

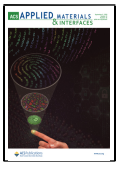

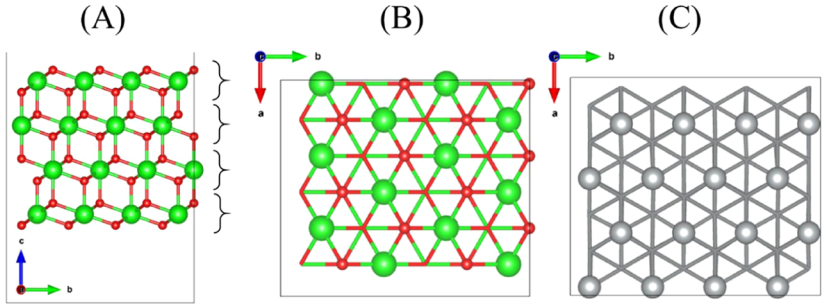

Figure 1. (A) Side view of the pristine $ZrO_2(111)$ slab in its bulk geometry. The (O−Zr−O) trilayers are shown between brackets. (B) Top view of the $ZrO_2(111)$ surface showing the top oxygen and zirconium layers with their hexagonal pattern. (C) Top view of the silver slab showing the hexagonal pattern of the (111) facet.

the adhesion properties. The nature of the terminal facet in contact does play a major role as it will strongly affect the chemical environment and, hence, the charge rearrangement at the interface.[24] For example, a metal oxide presenting an O-terminated surface such as the polar ZnO(000$\bar{1}$) facet has been shown to yield a stronger adhesion with silver compared to the corresponding Zn-terminated surface or the nonpolar facet, which has a stoichiometric amount of O/Zn at the surface.[15,25] However, the amplitude of the charge transfer is not always fully correlated with the difference in the work of adhesion when comparing several interfaces and, thus, cannot be used as a single indicator of the "quality" of the interface. This was earlier reported by Muñoz et al., who considered several body-centered cubic (bcc) and face-centered cubic (fcc) metals on zirconia and observed no direct correlation between the work of separation and the amount of charge transfer between the metal and oxygen atoms; however, the largest charge transfers were generally associated with the largest values of the work of separation.[15] In addition to the charge transfer, the nature of the interface bonding (*i.e.*, the degree of covalent character triggered by orbital hybridization) can be simultaneously exploited to increase the adhesion at interfaces.[25,26] In general, the theoretical studies considered clean interfaces in contact, while in reality some impurities can be present and can impact the charge transfer or lead to geometrical restructuration and, consequently, modify the work of adhesion. The decrease in interface strength due to impurities was demonstrated by Spencer et al. with sulfur impurities between the Fe(110) layers.[27] This destructive contribution also appears at mixed metal/oxide interfaces; Lin et al. investigated the impact of hydrogen adsorption on the ZnO/Ag interface and pointed to a decrease in the work of adhesion associated with local debonding.[28] More recently, the presence of interfacial water at a silica/resin interface was theoretically investigated, leading to the conclusion that the structural deformation of the hydrogen-bond network was the main mechanism of the adhesion loss.[29]

The doping of metal oxides is a well-known strategy to tune their electronic or mechanical properties.[30,31] This can be achieved by incorporating doping species inside the oxide or by modulating the oxide stoichiometry by generating defect vacancies, mainly in oxygen.[32] Nitrogen-doped or defective TiO_2 have been explored for photocatalysis applications,[33−37] and the structure/property relationship of doped or defective ZrO_2 has also been investigated.[38−42] In this respect, several DFT studies focused on the stability of the oxygen vacancies and their impact on the oxide properties.[38,43,44] Recently, Luo et al. have investigated the introduction of oxygen vacancy in ZrO_2 surfaces and have shown that oxygen vacancies are easier to generate on the (111) facet. In addition, they also described the effect of including a metallic dopant inside the oxide on the oxygen vacancy stability; over the 12 considered cations, only two (Ti and Pr) could promote the formation of the vacancy.[41] The stability of oxygen vacancies can also be controlled through the interfacial strain, as shown by Aidhy et al., who reported that a tensile-strain stabilizes the oxygen vacancies while they become less stable in a compressive interface.[45]

The doping approach opens many avenues to explore in the context of adhesion enhancement at oxide/metal interfaces. Indeed, including a dopant or changing stoichiometry is expected to affect the nature of the interface bonding and, hence, the work of adhesion. Theoretical studies have already addressed this issue and have indeed observed an enhancement in the adhesion energy at the interface when including a dopant inside one of the contact layers.[19] The chemical doping of an oxide layer mainly relies on a substitutional process in which oxygen atoms are replaced by other species. For example, the increase in the work of adhesion at oxide/metal interfaces can be promoted by substituting oxygen by a lower-vacancy atom such as nitrogen.[16] Recently, theoretical studies have also described the opposite approach, *i.e.*, substituting the metallic atom of the oxide to increase the interface adhesion. Li et al. have reported the impact of the valency state of the metallic atoms used as dopants at the SnO_2/Cu interface and demonstrated that low-valence dopants (such as Zn^{2+} or Cu^{2+}) enhance the interfacial adhesion while high vacancy dopants (such as Mo^{6+} or Sb^{5+}) act in an opposite way. This behavior is attributed to an excess of holes in the oxide consecutive to the low-valence doping, which promote a strong affinity for the electrons coming from the metallic layers.[21] Sun et al. have also investigated the effect of metallic dopant on the low-adhesive ZnO(0001)/ZrO_2(111) interface with a Zn-terminated surface. An increase in the work of adhesion was reported for yttrium-doped ZnO layers and was attributed to the mismatch reduction between the two oxides consecutive to the doping and by the segregation preference of the metallic dopant inside the oxide layer, leaving the interfacial zone intact.[46]

These large possibilities of the oxide improvement have motivated the present theoretical study aiming at assessing the impact on the poor adhesion that we reported for the ZrO_2(111)/Ag(111) interface of (i) n- or p-type doping of the oxide layer or (ii) point defects such as oxygen vacancies (V_O) and zirconium vacancies (V_{Zr}) alone or oxygen and zirconium vacancies together, either in a stoichiometric ratio (nV_{Zr} + $2nV_O$) or not.

https://dx.doi.org/10.1021/acsami.0c07579
ACS Appl. Mater. Interfaces 2020, 12, 40838−40849

2. METHODOLOGY

Quantum-chemical calculations were performed at the density functional theory (DFT) level with periodic boundary conditions, using the 4.1 version of the SIESTA code.[47] Exchange−correlation was described under the generalized gradient approximation (GGA) scheme using the Perdew−Burke−Ernzerhof (PBE) functional.[48] A numerical orbital basis set was used to describe the valence electrons, while core electrons were treated using Troullier−Martins pseudopotentials. The construction of the pristine ZrO_2/Ag interface consists of a layer-by-layer deposition of the silver (111) facet on the nonpolar (111) surface of ZrO_2 in an orthogonal unit cell of size 10.75 Å × 12.42 Å × 50.00 Å to ensure a good commensurability between the two lattices. Both silver and zirconium oxide surfaces were initially extracted from their bulk structure. The full system displays a thickness of five layers for silver and four ZrO_2 layers, each made of an (O−Zr−O) trilayer (Figure 1A). This represents a stoichiometry of $Zr_{48}O_{96}$ by the unit cell, with a total of 144 atoms for the zirconia surface in the pristine conditions. Both contact planes (oxide and silver) present a hexagonal pattern (Figure 1B,C). We focused here on the oxygen-terminated ZrO_2(111) surface as this facet is observed both theoretically and experimentally to be the most stable.[20,49−52] In addition, DFT works have already reported that maximizing the density of oxygen atoms facing the silver yields the best adhesive properties,[19] which further motivates the choice of a terminated-O facet.

The n- or p-type doping is realized in the pristine ZrO_2/Ag interface using the virtual crystal approximation (VCA),[53] *i.e.*, *via* a modification of the pseudopotential of oxygen or zirconium atoms, which proves efficient to address the impact of the doping.[54] The density of states (DOS) of the pristine ZrO_2 surface yields a valence [conduction] band dominated by O 2p [Zr 4d] orbitals (see Figure 2A). Therefore, the p-type doping was achieved by a small modification of the electronic configuration of the oxygen by removing on each atom a fraction of electron, while the n-type doping consists of adding a small fraction on each zirconium atom. The amount of electron density added or removed is quantified by considering an increase [decrease] by 1 electron for 100 zirconium [oxygen] atoms as equivalent to 1% doping. The electronic configurations used in this study are given in Table S1 in the Supporting Information.

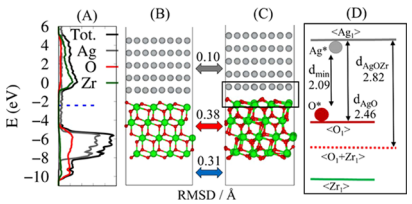

Figure 2. (A) Projected density of states (PDOS) of the pristine interface shown in (C). The position of the Fermi level is represented by a dashed line. Oxygen, zirconium, silver, and total contributions are represented in red, green, gray, and black, respectively. (B) Side view of the pristine ZrO_2/Ag interface (local relaxation, bottom layers fixed). (C) Side view of the pristine ZrO_2/Ag interface used in this study (full relaxation of the ZrO_2 layers). The amplitude of the atomic displacements from interface (B) to interface (C) is reflected by the root-mean-square-displacement (RMSD) value calculated on silver atoms only (gray arrow), oxide atoms only (red arrow), and over the whole structure (blue arrow). Oxygen, zirconium, and silver atoms are represented in red, green, and gray, respectively. (D) Schematic picture of the interface distance discussed in the text with their corresponding value (in angstrom) for the pristine case given in (C).

Neutral vacancies were introduced into the ZrO_2 layers by removing randomly and simultaneously n oxygen atoms (V_O, with n = 1, 2, 4, 8, 10, 16) and m zirconium atoms (V_{Zr}, with m = 1, 2, 4, 8) or by considering both oxygen and zirconium vacancies ($nV_O + mV_{Zr}$). For these, the chosen n/m ratio yields either stoichiometric (2:1 and 4:2) or nonstoichiometric (4:1 and 2:2) surfaces.

The geometries of the ZrO_2/Ag interfaces (with and without vacancies) were first fully optimized at the Γ-point with a mesh cutoff of only 250 Ry with the lattice parameters conserved to their pristine values. The atomic positions were relaxed using the conjugated gradient formalism until the forces were smaller than 0.04 eV $Å^{-1}$. The electronic properties were then calculated on these final geometries using a (5 × 4 × 1) Monkhorst−Pack grid with an increased mesh cutoff of 400 Ry. The charge density difference profiles were computed from the charge density of the full interface *versus* separated surfaces using the following equation

$$\rho_{diff} = \rho_{int} - [\rho_{Ag} + \rho_{ZrO_2}] \quad (1)$$

where ρ_{int} is the charge density of the ZrO_2/Ag interface and ρ_{Ag} and ρ_{ZrO_2} are the charge density of the silver layers and ZrO_2 layers in their relaxed geometry at the interface, respectively. From the total charge density of the VCA-doped systems, we computed the atomic charges using the Bader partitioning scheme.[55] This partition was also used for systems with vacancies in addition to the calculation of DDEC charges and effective bond order (EBO) using the DDEC/6 formalism.[56]

For each interface, the work of adhesion W has been calculated using the following equation

$$W = \frac{1}{A}[(E_{Ag} + E_{ZrO_2}) - E_{int}] \quad (2)$$

where E_{int}, E_{Ag}, and E_{ZrO_2} are the total energy of the Ag/ZrO_2 interface, silver surface, and zirconium oxide in their interface geometry, respectively, and A is the area of the contact surface. The transferred charge, Q_{Ag}, is mostly localized on the first silver layer in contact with the oxide surface and is defined as the average charge on the corresponding silver atoms, *i.e.*, $Q_{Ag} = 1/n\sum q_{Ag}$, with q_{Ag} being the silver atomic charges and n being the number of silver atoms per layer. The effective bond orders, EBOs, are also computed at the interface between all atomic pairs involving silver atoms and their closest neighbors (oxygen or zirconium) inside the oxide layer. We can next estimate the sum of the effective bond order (SEBO) for each individual silver atom and its connecting atoms. The averaged SEBO of the silver atoms localized in the contact plane is then calculated to provide a single metric quantifying the strength of the bonds at the interface; a value of 1 depicts the equivalent of a single chemical bond.

The relative stabilities of oxide surfaces containing defects can be compared in a formalism based on chemical potentials.[37] We first calculated the formation enthalpy of ZrO_2 as given in the following equation

$$\Delta H_f = [\mu_{Zr} - \mu_{Zr}(bulk)] + 2\left[\mu_O - \mu_O\left(\frac{1}{2}O_2\right)\right] \quad (3)$$

https://dx.doi.org/10.1021/acsami.0c07579
ACS Appl. Mater. Interfaces 2020, 12, 40838−40849

where μ_{Zr} and μ_O are the chemical potentials for zirconium and oxygen in the ZrO_2 bulk, respectively, and related by eq 4

$$\mu_{ZrO_2} = \mu_{Zr} + 2\mu_O \quad (4)$$

with μ_{ZrO_2} being the chemical potential of a ZrO_2 unit cell in the cubic ZrO_2 bulk computed as the total energy of the unit cell divided by the number (n = 4) of inequivalent ZrO_2 couples (μ_{ZrO_2} = −960.40 eV). μ_{Zr}(bulk) has been calculated in the hexagonal $P6_3/mmc$ bulk of zirconium as half the energy of the unit cell containing two atoms (μ_{Zr} = −80.44 eV), while $\mu(1/2\ O_2)$ = −432.92 eV is obtained as half the total energy of the dioxygen molecule isolated in a large periodic box. μ_O and μ_{Zr} differ depending on the synthetic conditions and the actual stoichiometric ratios, defining the so-called rich and poor conditions. To set an arbitrary reference value, in the case of O-rich conditions, we define $\mu_O = \mu(1/2\ O_2)$ and μ_{Zr} using eq 4. In our case, this leads to an enthalpy of formation of −13.91 eV. From this, we can next define the chemical potential limits from eq 3 as

$$\text{Zr} - \text{rich/O} - \text{poor conditions:}\ \ \mu_{Zr} = 0\ \text{eV};\ \ \mu_O = 1/2\ \Delta H_f = -6.95\ \text{eV} \quad (5.1)$$

$$\text{Zr} - \text{poor/O} - \text{rich conditions:}\ \ \mu_{Zr} = \Delta H_f = -13.91\ \text{eV};\ \ \mu_O = 0\ \text{eV} \quad (5.2)$$

The formation energy per point defect has been calculated for neutral vacancies as[37]

$$\Delta E_f = \frac{1}{(n+m)}[(E_V - E_0) + (n\mu_O + m\mu_{Zr}] \quad (6)$$

where E_V is the total energy of the system containing n vacancies in oxygen and m vacancies in zirconium and E_0 is the total energy of the pristine system. The reference energies for the missing oxygen or zirconium atoms are given by their corresponding chemical potential μ_O and μ_{Zr}, related by eq 4. We can rewrite the formation energy as a function of the oxygen chemical potential, leading to

$$\Delta E_f = \frac{1}{(n+m)}[(E_V - E_0 + m{\cdot}\mu_{ZrO_2})] + \frac{(n-2m)}{(n+m)}\mu_O \quad (7)$$

where μ_O varies between the two extreme limits described in expressions 5.1 and 5.2.

3. RESULTS AND DISCUSSION

3.1. Pristine ZrO_2(111)/Ag(111) Interface. Instead of freezing the bottom layers of ZrO_2 to their bulk geometry, as typically done,[52,57] we have here relaxed the full structure of the interface. This is to ensure a proper comparison with interfaces containing several vacancies that do require a complete geometry relaxation of the system. When starting from the cubic phase, the fully relaxed structure exhibits a displacement of the zirconium and oxygen atoms to adopt a structure close to a tetragonal symmetry (see Figure 2B,C). This reflects the polymorphic nature of zirconium oxide that yields less symmetric structures, *i.e.*, a monoclinic phase, at low temperature (below 1200 °C), while tetragonal and cubic phases prevail at high temperature (from ∼1200 to 2400 °C for the tetragonal phase and between 2400 and 2700 °C for the cubic phase).[58] Nevertheless, we chose to generate the interface from the cubic bulk structure to ensure a better commensurability with the silver layers and simplify the construction and characterization of the interface. Note that this approach can be justified by the possibility to effectively stabilize the tetragonal and cubic phases at low temperatures by synthetizing zirconia with additional cations (such as yttrium) or in substoichiometric conditions, introducing vacancies as dopants.[59−61] Moreover, this choice does not affect the main goal of our study, where the main focus is on the influence of doping and vacancies on adhesion energies with respect to a pristine system. When gluing the two facets and relaxing the structure, the magnitude of the geometric displacements of the atoms was characterized by calculating the root-mean-square-displacement (RMSD) between the initial and final structures. The value of the RMSD is 0.38 Å for the ZrO_2 layers, while the silver layers are quasi unaffected by the relaxation (RMSD of only 0.10 Å). The total RMSD of the whole interface system is calculated to be 0.31 Å. This indicates that the overall geometry of the zirconia/silver interface is not too much affected by the relaxation process. The main structural deformations are localized at the top layers of the oxide close to the interface. To analyze this region in deeper details, we have characterized the variation of the interfacial distance between the silver and ZrO_2 surfaces following eqs 8−10, see also Figure 2D:

$$d_{Ag-O} = \langle z_{Ag(1)}\rangle - \langle z_{O(1)}\rangle \quad (8)$$

$$d_{min} = z_{Ag^*} - z_{O^*} \quad (9)$$

$$d_{Ag-OZr} = \langle z_{Ag(1)}\rangle - \langle z_{O(1)} + z_{Zr(1)}\rangle \quad (10)$$

The definition given by eq 8 consists of calculating the difference along the z-direction between the average position of the silver atoms in the first layer, $\langle z_{Ag(1)}\rangle$, *i.e.*, those in contact with the metal oxide, and the average position of the oxygen atoms of the top layer of the oxide, $\langle z_{O(1)}\rangle$. This distance is labeled d_{Ag-O} in the remainder of the paper. However, to also account for a restructuration induced by doping of the surface or by the presence of one or more vacancies, we also introduced eq 9 to consider the difference between the vertical position of the silver atom closest to the oxide surface, z_{Ag^*}, and that of the oxygen atom closest to the silver layer, z_{O^*}. This definition entails a lower limit of the interfacial distance and is therefore labeled d_{min} in the paper. Note that these two definitions become equivalent in the case of two perfectly planar surfaces in contact. The difference between d_{Ag-O} and d_{min} is thus representative of the interface restructuration and the out-of-planarity character of the contact layers. Finally, to include possible displacements in the top zirconium layer, we also used eq 10 to define d_{Ag-OZr} that involves the average atomic position of both oxygen and zirconium atoms in the top ZrO bilayer ($\langle z_{O(1)} + z_{Zr(1)}\rangle$). Values of 2.09, 2.46, and 2.82 Å are obtained for d_{min}, d_{Ag-O}, and d_{Ag-OZr}, respectively, in the pristine interface. The difference of 0.35 Å between d_{min} and d_{AgO} underlines that the two planes in contact (the top oxygen layer and the silver layer) are not fully planar but present local distortions with some oxygen atoms moving down the zirconia layer while other oxygen atoms get closer to the silver layer and bind more strongly to the metal. This is nicely reflected through the effective bond order of the silver atoms that ranges from 0.28 to 0.50 depending on their relative position with respect to the oxygen atoms of the top oxide layer. Similarly, the intensity

https://dx.doi.org/10.1021/acsami.0c07579
ACS Appl. Mater. Interfaces 2020, 12, 40838−40849

and sign of the atomic charge of the individual silver atoms, q_{Ag}, strongly varies over the interfacial area. Indeed, despite a small average value of −0.035 |e|, the two extreme values of q_{Ag} are found to be −0.239 |e| for silver atoms facing oxygen atoms and +0.154 |e| in the case of silver atoms facing zirconium atoms. This behavior is rationalized from the difference in electronegativity between these atomic species (χ_O = 3.44; χ_{Zr} = 1.33; χ_{Ag} = 1.93). Between these extrema, values close to 0 are obtained for most of the silver atoms since they are localized in a bridge or hollow position with respect to the zirconia surface.

The work of adhesion amounts to 0.156 J m^{-2} in the fully relaxed interface (compared to 0.060 J m^{-2} initially calculated when the bottom two ZrO_2 layers are kept fixed). Despite this significant difference, the work of adhesion is still 1 order of magnitude less than that reported for other silver/metal oxide interfaces (*e.g.*, 2.0 J m^{-2} for polar ZnO(000$\bar{1}$)/Ag(111) interface). Since the average charge transfer (Q_{Ag}) and the sum of bond order (SEBO) have similar values in the two cases (see Table 1), the small increase in the work of adhesion obtained in the fully optimized case is mainly due to small structural changes, *i.e.*, a decrease in atomic separations at the interface when relaxing all layers of the metal oxide. As a matter of fact, the d_{min} distance calculated in the partially frozen interface model is 2.26 Å, to be compared to 2.09 Å obtained for the fully relaxed system. The new data reported in Table 1 will next be considered as our reference to assess the impact of doping the layers or introducing vacancies.

Table 1. Key Structural and Electronic Properties of the Pristine Ag/ZrO_2 Interface

	RMSD (Å)						
	total	ZrO_2	Ag	d_{min} (Å)	W (J m^{-2})	Q_{Ag} (|e|)	SEBO
ref 16	0.31	0.38	0.10	2.26	0.060	−0.044	0.35
this study				2.09	0.156	−0.035	0.37

3.2. Effect of Doping. We have first investigated the impact of doping the zirconia layers on the structural and electronic properties of the interface. Many dopants have been reported for zirconium oxide such as transition metal cations (Sc, Yb, Y), nitrogen atoms, or incorporated oxides.[60−63] Therefore, many structures could possibly be investigated by varying the nature of the dopant species, the position of the dopants inside the oxide (interstitial *versus* substitutional), or the dopant concentration. To provide a generic picture of the doping effect, we herein choose to use the virtual crystal approximation (VCA) approach. The n-type doping was achieved by artificially increasing the amount of electron per zirconium atom, while the p-type doping involves a modification of the valence electronic configuration of the oxygen atoms; this is done to reflect the fact that n-type dopants provide additional electrons to the ZrO_2 network, while the p-type dopants remove electrons. This approach is realistic at the low doping level, typically used in experiments, *i.e.*, in situations where we do not expect the physical introduction of dopants to be responsible for a significant structural modification of the ZrO_2 network.[54] The final geometries obtained after relaxation are shown in the Supporting Information (Figures S1 and S2). The actual restructuration of the interface upon electronic doping was quantified by the root-mean-square-displacement (RMSD) in the doped structures with respect to the pristine interface and by the evolution of the interfacial distances defined by eqs 8−10. For RMSD, we considered the displacement of all atoms in the system (total), the silver atoms only (silver), the zirconium oxide only (oxide), and finally the interfacial zone (interface), *i.e.*, layers Ag(1), O(1), and Zr(1). An increase in the atomic displacements is observed when increasing the amount of doping for both n- and p-type doping, though to a different extent, see Figure 3. Indeed, a quasi-linear evolution is obtained for n-type doping (Figure 3A), while p-type doping leads to small changes below 2% of doping and stronger atomic displacements beyond 2% (Figure 3B). The difference between the n- and p-type doping is also clear when focusing on the interfacial distances. For the n-type (Figure 3C), atomic restructuration mainly occurs at the interface and is accompanied by a large decrease in the d_{min} distance, implying that some oxygen or silver atoms are moving out of their respective layer. d_{Ag-ZrO} is also slightly reduced due to the global shift of the Zr(1) layer toward the interface. The average d_{AgO} distance remains globally constant, whatever the doping ratio, which is attributed to the absence of modification of the electronic valence of the oxygen atoms in contact with the silver layer, as we applied VCA on zirconium atoms only in the n-doped systems. This is not the case for p-type doping (Figure 3D) for which the d_{AgO} distance decreases from 2.46 Å (pristine) to 2.0 Å (at 10% doping). This distance is even lower than the d_{min} distance calculated for the pristine case (2.09 Å). The stronger modifications observed in the case of p-doping can be related to the nature of the oxide face exposed to silver. Indeed, since we consider here an O-terminated surface, the VCA applied to the oxygen atoms impacts the electronic valence of the chemical species directly in contact with the silver layers.

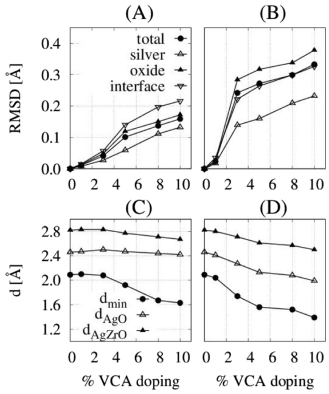

Figure 3. (Top) Evolution of the RMSD for n-doped (A) and p-doped (B) VCA doping as a function of the VCA ratio. (Bottom) Decrease in the interface distances defined in the text with the VCA doping for the n-doped (C) and p-doped (D) cases.

These geometric deformations have a large impact on the electronic properties of the interfaces. We report in Figure 4, the projected density of states for all doped interfaces in comparison to the pristine case. The initial band gap obtained for the pristine ZrO_2 is in the order of 3.0 eV. This value is relatively far from the experimental value of 5.4 eV but in the range of other theoretical values reported using GGA functionals that typically underestimate the band gap.[64] Although the DFT + U scheme was already successfully used to correct the band gap of zirconia,[39,65,66] this correction was

https://dx.doi.org/10.1021/acsami.0c07579
ACS Appl. Mater. Interfaces 2020, 12, 40838−40849

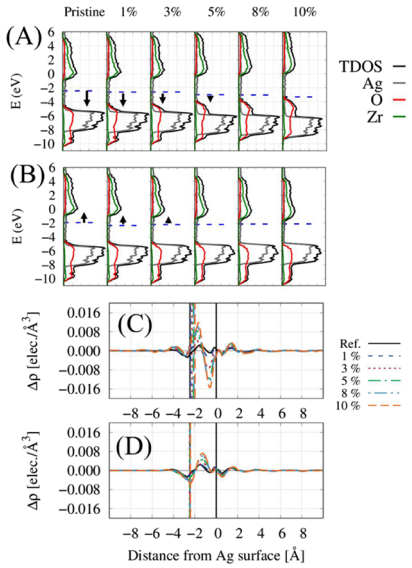

Figure 4. Projected and total density of states (TDOS) for p-doped (A) and n-doped (B) interfaces at each doping ratio. The partial density of states for oxygen, zirconium, and silver atoms are represented in red, green, and gray, respectively. The total density of states (TDOS) is in black. The position of the Fermi level is represented by a dashed line; black arrows depict the shift discussed in the main text. The charge density difference profile is also represented for p-doped (C) and n-doped (D) cases. The position of the silver contact layer has been set to 0. Negative distances correspond to the ZrO_2 layers, while positive distances are located inside the silver layers. Dashed lines correspond to the position of the top oxide layer.

not applied here as it does not affect the key quantities discussed in this work (see the last section of the Supporting Information). This band gap discrepancy is not a major issue when computing total energies in the ground state or when assessing the changes induced in the valence and conduction bands upon doping. As expected, p-doping (Figure 4A) induces a displacement of the Fermi level toward the valence band maximum (VBM), mainly composed of oxygen contributions. The Fermi level is initially localized 2.0 eV above the VBM in the pristine case (without doping) and gets in resonance with the VBM for a VCA doping of 10%. The opposite trend is obtained in the case of n-doping (Figure 4B), where the Fermi level, initially localized 1.0 eV below the conduction band minimum (CBM), shifts up in energy, reaching the CBM for a VCA doping of 10%.

The amount of charge transfer was calculated from a Bader charge analysis from which we extract the average atomic charge of silver Q_{av} in the contact plane Ag(1). The pristine interface used as reference points to a negligible interfacial charge transfer ($Q_{av} \sim 0.04$ |e|). The profile of the charge density difference for doped interfaces (Figure 4, bottom) shows that the direction of the charge transfer is correlated with the displacement of the VBM/CBM. In the case of p-doped zirconia, a large positive peak appears in the region corresponding to the top of the zirconia surface, while a negative peak of the same amplitude is localized in front of the silver layer. This points to a global charge transfer from the silver to the oxide. An opposite behavior is observed for n-doped zirconia, although with an amplitude reduced by one-third compared to the p-doped case for the largest peak. A similar trend is observed when looking at the evolution of the computed atomic charges. The n-doping case yields a negative Q_{av} value on the order of −0.1 |e| at 10% doping, while p-doping leads to a twice larger positive Q_{av} value (Figure 5). In

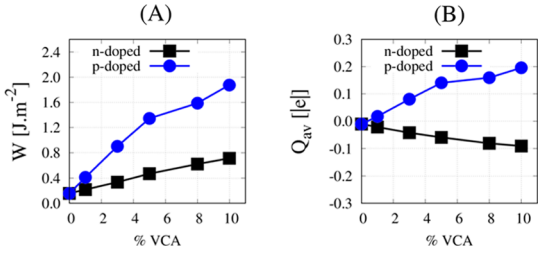

Figure 5. (A) Evolution of the work of adhesion, W, when increasing the virtual doping (VCA) ratio. (B) Evolution of the average atomic charge on silver Q_{av} when increasing the doping ratio. The n-doped (dark square) and p-doped (blue circle) systems were generated at the VCA level by a modification of the zirconium and oxygen pseudopotential, respectively.

turn, these interfacial charge transfer processes have a strong impact on the work of adhesion, showing an increase from 0.156 J m^{-2} (pristine) up to 0.800 J m^{-2} for 10% n-doped systems. The effect is even more intense for p-type doping with adhesion energies at 10%, reaching 1.9 J m^{-2}, *i.e.*, a value similar to the largest adhesion energy obtained in our previous studies for polar oxide surfaces. The systematic increase in the adhesion energy is rationalized by the increased ionic character of the interfacial bonding.

3.3. Effect of Vacancies. The effect of vacancies has been investigated for structures, including oxygen vacancies (V_O), zirconium vacancies (V_{Zr}), and mixed vacancies (V_O + V_{Zr}). Several studies have been reported for defect vacancies in the bulk and at surfaces of zirconia considering neutral, positive, or negative defect centers.[67−69] Since we expect charges to be ultimately neutralized in devices, we focus here on neutral vacancies only. The position of the vacancies inside the oxide was selected semirandomly by ensuring that no vacancies are localized at the interfacial area. The reason for this is to investigate the effect of bulk vacancies on the work of adhesion and the amount of charge transferred. Moreover, this also prevents silver intercalation into the oxide, which could generate more complex structures beyond the scope of this study. The final geometries obtained after relaxation for each case are shown in the Supporting Information (Figures S3−S5). The interface of all structures has been characterized by the interface distances and RMSD, as done before for the doped interfaces (Figure 6). They will be described for each case in the next subsections.

3.3.1. Oxygen Vacancies (V_O). First, we have considered the presence of oxygen vacancies in the ZrO_2 layers. Starting from the pristine interface and keeping the system electronically neutral, we have generated vacancies by randomly removing 1 up to 16 oxygen atoms out of the 96 atoms contained in our ZrO_2 slab, *i.e.*, an atomic vacancy doping going from ∼1 to ∼16%. The full interface was then relaxed following the procedure described in Section 2. Figure 6 shows that a large geometric restructuration is observed in the presence of oxygen vacancies. This translates into RMSD values that can reach 0.8 Å for a high number of vacancies. The interface distance d_{min} tends to decrease with the number of vacancies down to 1.1 Å, which indicates that some oxygen atoms of the top layer of zirconia leave their initial plane; this also holds true for the

https://dx.doi.org/10.1021/acsami.0c07579
ACS Appl. Mater. Interfaces 2020, 12, 40838−40849

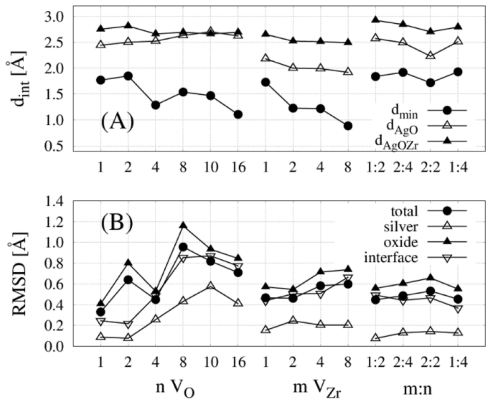

Figure 6. (A) Evolution of the three interface distances discussed in the text, d_{min} (circle), d_{AgO} (empty triangle), and d_{AgOZr}, (filled triangle) when increasing: (i) the number of oxygen vacancies V_O (first series of points); (ii) the number of zirconium vacancies V_{Zr} (second series of points); and (iii) by mixing oxygen and zirconium vacancies (last series). (B) Evolution of the RMSD as defined in the text when increasing: (i) the number of oxygen vacancies V_O; (ii) the number of zirconium vacancies V_{Zr}; and (iii) by mixing oxygen and zirconium vacancies.

silver atoms in view of the RMSD value for silver atoms that strongly increases with the number of oxygen vacancies, reaching values in the range of 0.4−0.6 Å for a high density of V_O. The two other characteristic distances, d_{Ag-O} and d_{Ag-OZr} follow a different trend. Surprisingly, the distance d_{Ag-O}, reflecting the average separation between the two contact layers, slightly increases in a linear way with the number of vacancies, while d_{Ag-OZr} accounting for the first zirconium layer slightly decreases to reach a value close to d_{Ag-O} at high V_O density. This behavior is explained by a large restructuration inside the zirconia layer triggered by a large number of vacancies. As a matter of fact, to avoid the presence of unpaired electrons, a reordering of the layer is observed. This restructuration is clearly observed in Figure 7, reporting the

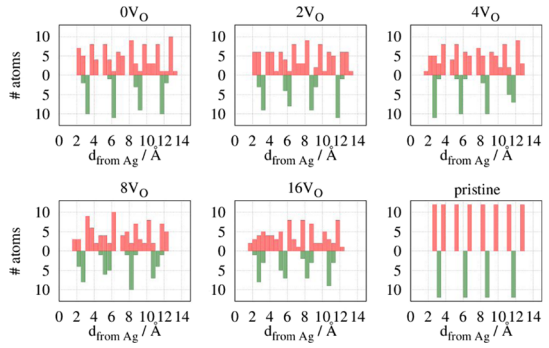

Figure 7. Atomic distribution inside the ZrO_2 layers for the several ZrO_2 + nV_O oxide surfaces. The number of oxygen atoms (red) and zirconium atoms (green) is reported as a function of the distance from the silver layers by a step of 0.5 Å. The pristine ZrO_2 oxide in the absence of silver is also shown for comparison.

atomic distribution as a function of the distance with respect to the silver surface (*i.e.*, the number of atoms by a slice of 0.5 Å). The reference system (without vacancy) exhibits a distribution shape highlighting the O−Zr−O ordering inside the oxide. This reference structure already presents some restructuration consecutive to the silver adsorption as the 12 facing oxygen atoms are not equally distributed as it is the case in the bare ZrO_2 slab, see Figure 7. A similar behavior appears inside the zirconium layers with a fraction of zirconium atoms moving away from their bulk position. By comparison, the structure containing 16 V_O presents a massive restructuration as evidenced by the quasi-uniform distribution of oxygen atoms in the area close to the silver surface (*i.e.*, between 2.0 and 4.5 Å from the surface).

The introduction of oxygen vacancies also impacts the electronic structure of the interface manifested through a shift of the Fermi level toward the CBM (mainly governed by zirconium) characteristic of n-type doping; the density of states also features the appearance of states with contributions from Zr and O atoms below the Fermi level, see Figure 8A,B. The

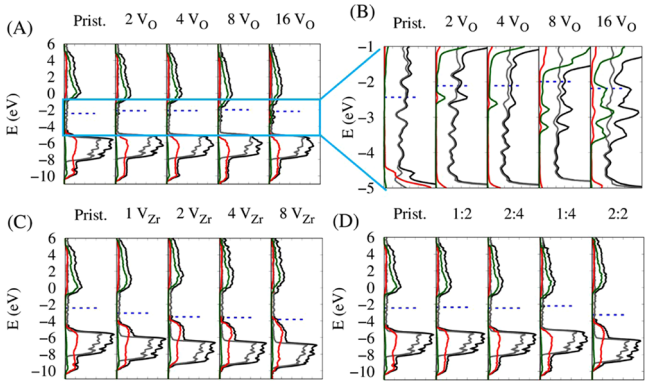

Figure 8. Projected density of states (PDOS) for the interfaces with vacancies. (A) Oxygen vacancies, (B) oxygen vacancies with a zoom on the gap state area, (C) zirconium vacancies, and (D) zirconium and oxygen vacancies. PDOS for silver, oxygen, and zirconium are represented in gray, red, and green, respectively. The total DOS is in black. The Fermi level is represented by a dashed line.

presence and localization at 2.0 eV above the VBM of such localized states induced by the vacancies are consistent with what has already been theoretically reported for a neutral V_O vacancy in the bulk and at the surface of zirconia.[67−69] Similar results were also reported for a single V_O inside TiO_2 and related to the formation of Ti 3d states consecutive to a $Ti^{4+} \rightarrow Ti^{3+}$ reduction due to charge imbalance. A deeper analysis of the gap states reveals the same behavior here. Indeed, the gap states are generated by the hybridization of 4d orbitals of two Zr atoms, which get closer upon layer reconstruction. Note that this change appears to be associated with local effects as increasing the number of oxygen vacancies does not lead to a systematic increase in the density of such specific states. Recent theoretical studies have also reported the possibility of manipulating spin polarization in oxides by generating vacancies.[70,71] Although this process relies on the removal of a metallic atom, we have briefly considered this aspect here by applying a spin-polarized calculation for our $4V_O$ interface geometry. Interestingly, we observe a significant spin polarization only for the two hybridized zirconium atoms described above, with an atomic spin moment (asm) of −0.82 and −0.71 μ_B (a third closely lying zirconium atom also displays an asm value of −0.18 μ_B). The other atoms remain unaffected or have an |asm| lower than 0.07 μ_B, which indicates that it is mainly the local restructuration and atomic hybridization induced by the vacancy that drives the induced atomic spin moment rather than the concentration of vacancy. This observation is consistent with experimental results obtained on TiO_2 samples

https://dx.doi.org/10.1021/acsami.0c07579
ACS Appl. Mater. Interfaces 2020, 12, 40838−40849

indicating that even a decrease in the spin polarization can be observed in the presence of a too large number of vacancies; this behavior is attributed to the formation of clusters of vacancies.[70]

The introduction of vacancies induces a charge transfer from the oxide into the silver that evolves in amplitude in a quasi-linear way for a small number of vacancies (less than 8%) and saturates at higher ratios (Figure 9). This is nicely correlated

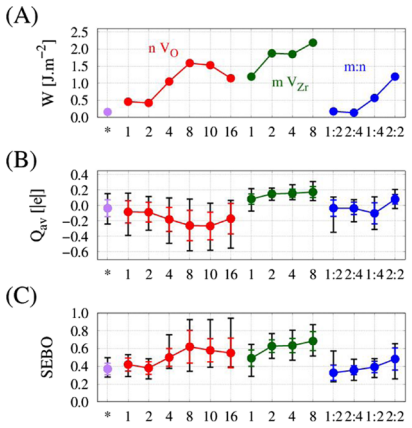

Figure 9. Investigated interfacial properties for the ZrO_2/Ag interface as a function of the number of vacancies in oxygen atoms nV_O (red points), in zirconium atoms mV_{Zr} (green points), or when mixing nV_O and mV_{Zr} vacancies (blue points). The calculated values for the pristine case (*) are given in purple for comparison. (A) Calculated work of separation, *W*. (B) Average charges on the silver atoms facing the oxide surface atoms (filled dot). (C) Sum of effective bond order, SEBO, (filled dot). For these two last quantities, the minimum and maximum values in the data distribution are represented by black error bars, while the color error bars represent the standard deviations of the distribution.

with the evolution of the work of adhesion, which increases linearly from 0.15 J m^{-2} up to more than 1.5 J m^{-2} at 8% of vacancies in oxygen before reaching a plateau at higher values. This transition can be associated with the increase in the disorder at the interface area, as reflected by the linear increase in the interface RMSD but also by a larger dispersion of the data, especially the bond orders (see error bars in Figure 9), for the oxide with four of more oxygen vacancies.

3.3.2. Zirconium Vacancies (V_{Zr}). Similar to the procedure described above, we generate here random vacancies in zirconium by removing one, two, four, and eight atoms inside the oxide layers. The distance d_{AgO} slightly decreases with a growing number of vacancies and goes down below 2.0 Å for V_{Zr} = 8; the same trend prevails for d_{min} though the drop occurs in a larger extent down to ca. 0.9 Å for V_{Zr} = 8, which underlines a strong degree of restructuration of the oxide contact plane, with the oxygen atoms moving closer to the silver layer. In contrast to the V_O case, both d_{AgO} and d_{AgOZr} display a parallel evolution evidencing that the geometric restructuration occurs in a more cooperative way; in other words, all ZrO_2 layers move closer to the silver layer with less internal restructuration inside the zirconia layer. This is further supported by the evolution of the RMSD that slowly increases in the presence of V_{Zr} compared to V_O. The RMSD of the silver atoms stays on the order of 0.2 Å, whatever the number of V_{Zr}, thus pointing as well to a weak internal restructuration. This behavior is also reflected by the smaller dispersion of the interfacial parameters (silver charges and SEBO) compared to the V_O cases, as seen in Figure 9, where the standard deviation and extreme values are reported.

The impact of V_{Zr} vacancies on the electronic structure of the interface is shown in Figure 8. We observe a shift of the Fermi level toward the valence band edge localized on the oxygen in a way similar as for p-type doping (see the previous section). In contrast to V_O, no gap states are observed in the presence of V_{Zr}. The introduction of zirconium vacancies induces a charge transfer in the opposite direction compared to the oxygen vacancies, with the accumulation of positive charges in the silver plane. The evolution of the charge transfer with the density of vacancies is represented in Figure 8; there are two distinct regimes, with first an increase in the charge transfer with a small number of vacancies (V_{Zr} = 1−2) followed by a saturation limit after V_{Zr} = 4. This trend is fully reproduced when calculating the work of adhesion, with a strong linear increase from 0.156 J m^{-2} (V_{Zr} = 0) up to ca. 2.0 J m^{-2} (V_{Zr} = 2), followed by a plateau for a yet higher number of vacancies; this correlation fully demonstrates that the increase in the work of adhesion is driven by the Coulomb attraction between the charges of the opposite sign at the two sides of the interfaces. Combining now the results obtained for V_O and V_{Zr}, we are led to the conclusion that the presence of a single type of vacancies has a large positive impact on the strength of adhesion. This further indicates that it is the intensity of the charge transfer rather than its direction (from metal to oxide or *vice versa*) that drives the improvement in the adhesion properties. Moreover, the Zr vacancies are found to have a stronger impact on the adhesive properties than V_O. This trend is actually observed for both homo and mixed vacancies (*vide infra*). We can use as indicators of a good adhesion: (a) the magnitude of the interfacial charge transfer; (b) the bond order (SEBO); and (c) the average interfacial distance. Although these parameters are closely related, we demonstrated that they can act constructively or destructively depending on the nature of the oxide layer (atomic species, polar *versus* nonpolar facet).[16] For the sake of illustration, polar (000$\bar{1}$) ZnO and (001) ZrO_2 surfaces combine both a large charge transfer and bond order with the silver layers, as reflected by their high adhesion energies (2.0−3.0 J m^{-2}) while nonpolar (10$\bar{1}$0) ZnO has a high bond order but a very weak charge transfer with silver, leading to a reduction by a factor 2 with respect to the polar case. In the present study, V_{Zr}- and V_O-based systems display the same general trend with first a linear evolution of the charge transfer and SEBO with the number of vacancies followed by a saturation plateau (Figure 9). For V_O-based systems, the transition between these two regimes appears after four vacancies in oxygen (∼4% of vacancy doping). V_{Zr}-based systems adopt the same behavior at the same doping value limit when taking into account the stoichiometry since the saturation is reached after two vacancies in zirconium. At a high concentration of vacancies (up to 4%), similar charge transfer amplitudes Q_{Ag} (with opposite direction) and similar SEBO are obtained for both V_{Zr}- and V_O-based systems. For V_O, Q_{Ag} is between −0.2 and −0.3 |e| with a maximum SEBO of ∼0.55, see Figure 9. In the case of V_{Zr}, the absolute value of the charge transfer is slightly reduced (∼0.2 |e|) but is compensated by a higher SEBO with values between 0.65 and 0.70 for a high concentration of V_{Zr}. However, the main difference appears in the geometry reorganization at the interface, especially in the behavior of the average interface distance, d_{Ag-O}. In the case of oxygen vacancies, a large restructuration occurs at the interface area (see Figure 6)

https://dx.doi.org/10.1021/acsami.0c07579
ACS Appl. Mater. Interfaces 2020, 12, 40838−40849

though d_{AgO} stays globally constant around 2.5−2.6 Å. In the case of V_{Zr} vacancies, local reconstructions also take place (as evidenced from the RMSD evolution and d_{min} distance) but with a linear decrease in the average interfacial distance below 2.0 Å at high V_{Zr} concentration. This variation by 0.5 Å of the interface distance coupled to a similar charge transfer and bond order can explain the stronger adhesive properties of V_{Zr}-compared to V_O-based interfaces. One might have expected this difference in the interface distances to be reflected in the values of charge transfer and bond order displayed in Figure 9. However, the local structural effects that appear only in the V_{Zr}-based systems (with oxygen atoms moving very close to the interface area) do contribute to increase the work of adhesion although hidden when presenting the average data collected in Figure 9.

3.3.3. Mixed Vacancies (V_O + V_{Zr}). We now consider the presence of both oxygen and zirconium vacancies inside the oxide layer by first considering a stoichiometric ratio. More precisely, we have calculated two interface structures with one ($1V_{Zr}$ + $2V_O$) and two ($2V_{Zr}$ + $4V_O$) missing ZrO_2 unit(s) in the oxide layer, with V_O and V_{Zr} randomly distributed. The calculated projected density of states show that no modification in the electronic structure is observed in these specific conditions. Similarly, the work of adhesion calculated on these two interface structures slightly varies compared to the reference pristine interface (W = 0.156 J m^{-2}), with W of 0.173 J m^{-2} for ($1V_{Zr}$ + $2V_O$) and 0.136 J m^{-2} for ($2V_{Zr}$ + $4V_O$). The analysis of the charge transfer and bond order reveals that the presence of a stoichiometric number of V_O and V_{Zr} vacancies has no influence on the charge density profile and yields only a tiny change in the bond order. These results thus indicate that improving adhesive properties requires the oxide to be out of stoichiometry. To fully confirm this, we have generated two other structures containing: (i) an excess of oxygen vacancies with a 1:4 ratio ($1V_{Zr}$ + $4V_O$) and (ii) an excess of zirconium vacancies with a 2:2 ratio ($2V_{Zr}$ + $2V_O$). The analysis of the resulting ZrO_2/Ag interface shows that the variation in the characteristic interface distances is consistent with the evolutions observed with homo-vacancies for the species in excess. Indeed, the system containing an excess of V_O displays an interface distance d_{Ag-O} of 2.50 Å that is similar to the distance computed for the interface with one or two V_O vacancy(ies). In the opposite case (*i.e.*, an excess of V_{Zr}), a decrease in the interface distance d_{Ag-O} down to 2.2 Å is observed, as it is the case with V_{Zr} vacancies alone. The modification of the V_{Zr}/V_O ratio also has an impact on the electronic structure. Going out of stoichiometry modifies the projected density of states in a similar way as single vacancies do, namely, with a displacement of the valence band edge and the appearance of gap states for the 1:4 system (as observed for V_O) and a displacement of the conduction band edge for the 2:2 system (as observed for V_{Zr}), see Figure 8. As a consequence, an excess of one type of vacancy strongly impacts also the calculated work of adhesion. For the ($1V_{Zr}$ + $4V_O$) and ($2V_{Zr}$ + $2V_O$) systems, the work of adhesion is calculated to be 0.564 and 1.193 J m^{-2}, respectively; these two values are fully consistent with those obtained for homo-vacancies, with V_{Zr} having a stronger impact on the work of adhesion than V_O. The profiles of charge density difference also evidence the inversion of the charge transfer direction when changing the V_{Zr}/V_O ratio, as discussed before for the homo-vacancy cases.

3.4. Formation Energies. Previous sections have described the impact of introducing vacancies on the work of adhesion and have pointed to a stronger impact of V_{Zr} compared to V_O. Here, we discuss the calculated formation energies of the different defects to assess whether some are more favored than others from a thermodynamic perspective. The calculations have been performed on the bare oxide surface using the procedure described in Section 2. The results are given in Figure 10, where we report the evolution of the

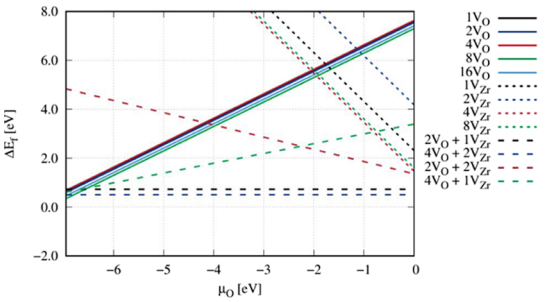

Figure 10. Evolution of the formation energy per vacancy calculated in the free oxide surface as a function of the oxygen chemical potential. The density of oxygen vacancies increases when varying μ_O from the right side to the left side of the graph.

formation energies with respect to the oxygen chemical potential ranging between the rich and poor conditions given by expressions 5.1 and 5.2. The formation of neutral oxygen vacancies appears to be favored in poor oxygen conditions with a small impact of the actual number of vacancies, while neutral zirconium vacancies are less stable even at zirconium poor conditions (oxygen-rich, μ_O = 0). This points to a preferred formation of oxygen vacancies rather than zirconium vacancies in such structures, which was also reported theoretically for cubic bulk zirconia and in a surface slab of zirconia.[69] For the mixed-vacancy cases, the two stoichiometric ratios ($2V_O$ + V_{Zr} and $4V_O$ + $2V_{Zr}$, where m = $n/2$) make expression 9 independent of the oxygen chemical potential and correspond to the most stable defective defects. These two systems are less stable than the pristine case with ΔE_f of +0.72 and +0.50 eV for $2V_O$ + V_{Zr} and $4V_O$ + $2V_{Zr}$, respectively. When going out of stoichiometry, an excess of zirconium vacancy ($2V_O$ + $2V_{Zr}$) is unstable whatever the chemical potential, while an excess of oxygen vacancy ($4V_O$ + $1V_{Zr}$) leads to a decrease in ΔE_f in poor oxygen conditions. This is consistent with the behavior observed in the case of homo-vacancies and the preference for lacunar defects in oxygen rather than in zirconium. Altogether, starting from a given oxygen chemical potential (or stoichiometric ratio), this graph demonstrates that several defects can be created in parallel depending on the input energy received by the sample.

The thermodynamic conditions that stabilize interfaces with oxygen vacancies can be described in first approximation by introducing a dependence on pressure and temperature in the definition of the oxygen chemical potential as follows

$$\mu_O(T, p) = \left[\frac{1}{2}E_{O_2} + k_B T \log\left(\frac{p}{p^0}\right)\right] \quad (11)$$

where T and p are the temperature and pressure of the oxygen gas, k_B the Boltzmann constant, and p^0 the atmospheric

https://dx.doi.org/10.1021/acsami.0c07579
ACS Appl. Mater. Interfaces 2020, 12, 40838−40849

pressure. From this expression, we can define the surface energy as

$$\gamma(T, p) = \frac{1}{A}[E_{tot} - E_{Ag} - E_{ZrO_2} + n_O\mu_O(T, p)] \quad (12)$$

with E_{tot} being the total energy of the interface and E_{Ag}/E_{ZrO_2} being the total energy of the silver and oxide layer in their pristine conditions. Under this form, expression 12 corresponds, when no vacancy is introduced in the system ($n_O = 0$), to the commonly used expression of the surface energy and has an opposite sign with respect to the calculated work of adhesion discussed before ($\gamma = -0.156$ J m^{-2}). When working at atmospheric pressure ($p = p^0$), the contribution of the chemical potential is independent of temperature and takes its maximal value corresponding to $1/2\,E_{O_2}$ (our zero reference for μ_O). Based on the data given in Figure 10, the formation energy of defect is highly unfavorable under these conditions. Indeed, the calculated γ for the interface with one oxygen vacancy at p^0 is larger by 0.6 J m^{-2} with respect to the pristine case. The stabilization of this interface can be achieved by working at low gas pressure and/or high temperature. In Figure 11, we reported the calculated temperature/pressure

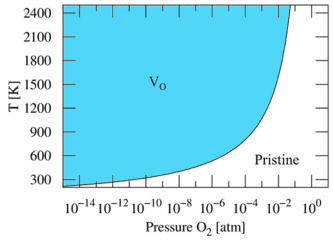

Figure 11. Thermodynamic diagram showing the stability of the interface with one oxygen vacancy with respect to the pristine case for a given range of temperatures and pressures of the O_2 gas.

diagram for the pristine interface *versus* the interface with one oxygen vacancy. On that basis, the pristine interface appears to be more stable under a large range of temperatures when working at pressure between 10^{-1} and 1 atm. Below 10^{-2} atm and for high temperature, the interface with one vacancy is stabilized and will be the preferential one at room temperature at very low pressure (<10^{-9} atm).

4. CONCLUSIONS

In this study, we computed by means of a periodical quantum-chemical approach the change in the adhesive properties (work of adhesion, W) of a metal oxide/silver interface, *i.e.*, the $ZrO_2(111)/Ag(111)$ interface, when introducing dopants or vacancies. We focused on this interface because, despite the advantages of using zirconia, it exhibits a very low work of adhesion in the pristine state and is thus prone to the largest improvements. To study the doping effects, we adopted the VCA approach and modeled n-type and p-type-doped zirconia. Both types of doping have been shown to strongly affect the adhesive properties, with an increase in the work of adhesion up to 0.8 J m^{-2} (n-type) and 2.0 (p-type) J m^{-2} at a high doping ratio (10%); such values are comparable to those obtained at the same level of theory for the most adhesive polar oxide surfaces such as ZnO. On the other hand, we have considered vacancies in oxygen atoms (V_O), zirconium atoms (V_{Zr}), and mixed vacancies (V_O + V_{Zr}), in stoichiometric or nonstoichiometric ratios. Our calculations show that the presence of vacancies strongly affects the adhesive properties of silver onto the oxide with a linear increase in W at a small number of vacancies (~4% and less) before reaching a saturation plateau at higher concentrations. The value of the work of adhesion at this saturation limit has the same order of magnitude as the value obtained for the n/p-doped case, with $W \sim 1.5$ J m^{-2} for V_O and $W \sim 2.0$ J m^{-2} for V_{Zr}. The stoichiometric cases do not show any increase in the work of adhesion compared to the pristine ZrO_2/Ag interface, which indicates that this effect is purely connected to the presence of an excess of vacancies of one kind acting as doping centers. Indeed, the two nonstoichiometric cases yield similar results than those obtained assuming homo-vacancies in the species in excess. The calculation of the formation energy of defects within the oxide layers of various starting stoichiometries (or oxygen chemical potentials) shows that the presence of neutral V_{Zr} inside the layer is typically not favored (although it is calculated as the best scenario in terms of strong adhesive properties). However, neutral V_O also yields good adhesive properties with high stability in poor oxygen conditions and, thus, appear to be the ideal candidate to increase adhesive properties in oxide/silver interfaces presenting poor adhesion in their pristine form. These results demonstrate that "poor" interfaces in term of work of adhesion can be strongly improved by a fine-tuning of the oxide layer *via* dopants or vacancies. This approach can thus increase the number of potential materials in the development of new low-e glasses. Implementing chemical modifications in an oxide material for adhesion enhancement while conserving its other native properties (such as stress resistance or chemical stability, *etc.*) might, however, be challenging. This opens the way for further theoretical and experimental investigations.

■ ASSOCIATED CONTENT

Supporting Information

The Supporting Information is available free of charge at https://pubs.acs.org/doi/10.1021/acsami.0c07579.

Pseudopotential configurations used for the VCA approximation; pictures of the final relaxed interfaces and Table with the location of the vacancies; CIF coordinates of the output structures discussed in the manuscript; table of the interface distances and oxide bond lengths; distribution of the Zr−O bond length inside the oxide layers for each interface; comparison between DFT and DFT + U for selected interfaces (PDF)

■ AUTHOR INFORMATION

Corresponding Author

Jérôme Cornil − *Laboratory for Chemistry of Novel Materials, University of Mons (UMONS), 7000 Mons, Belgium;* orcid.org/0000-0002-5479-4227; Email: jerome.cornil@umons.ac.be

Authors

David Cornil − *Laboratory for Chemistry of Novel Materials, University of Mons (UMONS), 7000 Mons, Belgium;* orcid.org/0000-0002-9553-1626

Nicolas Rivolta − *AGC Glass Europe Technovation Centre, 6041 Gosselies, Belgium*

https://dx.doi.org/10.1021/acsami.0c07579
ACS Appl. Mater. Interfaces 2020, 12, 40838−40849

Virginie Mercier − *AGC Glass Europe Technovation Centre, 6041 Gosselies, Belgium*
Hughes Wiame − *AGC Glass Europe Technovation Centre, 6041 Gosselies, Belgium*
David Beljonne − *Laboratory for Chemistry of Novel Materials, University of Mons (UMONS), 7000 Mons, Belgium;* orcid.org/0000-0002-2989-3557

Complete contact information is available at: https://pubs.acs.org/10.1021/acsami.0c07579

Notes

The authors declare no competing financial interest.

■ ACKNOWLEDGMENTS

This research was supported by AGC Glass Europe and the Région Wallonne. Computational resources were provided by the Consortium des Équipements de Calcul Intensif (CÉCI), funded by the Fonds National de la Recherche Scientifique de Belgique (F.R.S.-FNRS) under Grant 2.5020.11. J.C. and D.B. are FNRS research directors.

■ REFERENCES

(1) Aguilar-Santana, J. L.; Jarimi, H.; Velasco-Carrasco, M.; Riffat, S. Review on window-glazing technologies and future prospects. *Int. J. Low-Carbon Technol.* **2020**, *15*, 112−120.
(2) Jelle, B. P.; Kalnæs, S. E.; Gao, T. Low-emissivity materials for building applications: A state-of-the-art review and future research perspectives. *Energy Build.* **2015**, *96*, 329−356.
(3) Barthel, E.; Kerjan, O.; Nael, P.; Nadaud, N. Asymmetric silver to oxide adhesion in multilayers deposited on glass by sputtering. *Thin Solid Films* **2005**, *473*, 272−277.
(4) Alvarez, R.; González, J. C.; Espinós, J. P.; González-Elipe, A. R.; Cueva, A.; Villuendas, F. Growth of silver on ZnO and SnO_2 thin films intended for low emissivity applications. *Appl. Surf. Sci.* **2013**, *268*, 507−515.
(5) Ando, E.; Miyazaki, M. Durability of doped zinc oxide/silver/doped zinc oxide low emissivity coatings in humid environment. *Thin Solid Films* **2008**, *516*, 4574−4577.
(6) Kulczyk-Malecka, J.; Kelly, P. J.; West, G.; Clarke, G. C. B.; Ridealgh, J. A.; Almtoft, K. P.; Greer, A. L.; Barber, Z. H. Investigation of silver diffusion in TiO_2/Ag/TiO_2 coatings. *Acta Mater.* **2014**, *66*, 396−404.
(7) Akin Sonmez, N.; Donmez, M.; Comert, B.; Ozcelik, S. Ag/M-seed/AZO/glass structures for low-E glass: Effects of metal seeds. *Int. J. Appl. Glass Sci.* **2018**, *9*, 383−391.
(8) Shahidi, M. M.; Rezagholipour Dizaji, H.; Ehsani, M. H.; Ghazi, M. E. Effect of GLAD technique on optical and electrical properties of SnO_2/Ag/SnO_2 structure. *Infrared Phys Technol.* **2020**, *106*, No. 103263.
(9) Chevalier, J.; Gremillard, L.; Virkar, A. V.; Clarke, D. R. The Tetragonal-Monoclinic Transformation in Zirconia: Lessons Learned and Future Trends. *J. Am. Ceram. Soc.* **2009**, *92*, 1901−1920.
(10) Özcan, M.; Volpato, C. A. M. Adhesion to Zirconium Dioxide Used for Dental Reconstructions: Surface Conditioning Concepts, Challenges, and Future Prospects. *Curr. Oral Health Rep.* **2015**, *2*, 190−194.
(11) Thompson, J. Y.; Stoner, B. R.; Piascik, J. R.; Smith, R. Adhesion/cementation to zirconia and other non-silicate ceramics: Where are we now? *Dent. Mater.* **2011**, *27*, 71−82.
(12) Sinhamahapatra, A.; Jeon, J.-P.; Kang, J.; Han, B.; Yu, J.-S. Oxygen-Deficient Zirconia (ZrO_{2-x}): A New Material for Solar Light Absorption. *Sci. Rep.* **2016**, *6*, No. 27218.
(13) Gogotsi, G. A.; Lomonova, E. E.; Pejchev, V. G. Strength and fracture toughness of zirconia crystals. *J. Eur. Ceram. Soc.* **1993**, *11*, 123−132.
(14) Guo, X. Property Degradation of Tetragonal Zirconia Induced by Low-Temperature Defect Reaction with Water Molecules. *Chem. Mater.* **2004**, *16*, 3988−3994.
(15) Muñoz, M. C.; Gallego, S.; Beltrán, J. I.; Cerdá, J. Adhesion at metal-ZrO_2 interfaces. *Surf. Sci. Rep.* **2006**, *61*, 303−344.
(16) Cornil, D.; Wiame, H.; Lecomte, B.; Cornil, J.; Beljonne, D. Which Oxide for Low-Emissivity Glasses? First-Principles Modeling of Silver Adhesion. *ACS Appl. Mater. Interfaces* **2017**, *9*, 18346−18354.
(17) Anagnostopoulos, G.; Sygellou, L.; Paterakis, G.; Polyzos, I.; Aggelopoulos, C. A.; Galiotis, C. Enhancing the adhesion of graphene to polymer substrates by controlled defect formation. *Nanotechnology* **2018**, *30*, No. 015704.
(18) Lin, Z.; Bristowe, P. D. Microscopic characteristics of the Ag(111)/ZnO(0001) interface present in optical coatings. *Phys. Rev. B* **2007**, *75*, No. 205423.
(19) Phillips, C. L.; Bristowe, P. D. First principles study of the adhesion asymmetry of a metal/oxide interface. *J. Mater. Sci.* **2008**, *43*, 3960−3968.
(20) Cadi-Essadek, A.; Roldan, A.; de Leeuw, N. H. Ni Deposition on Yttria-Stabilized ZrO_2(111) Surfaces: A Density Functional Theory Study. *J. Phys. Chem. C* **2015**, *119*, 6581−6591.
(21) Li, W.-J.; Shao, W.-Z.; Chen, Q.; Zhang, L.; Han, Y.; Chen, B.-A.; Wang, Q.; Zhen, L. Effects of dopants on the adhesion and electronic structure of a SnO_2/Cu interface: a first-principles study. *Phys. Chem. Chem. Phys.* **2018**, *20*, 15618−15625.
(22) Popov, M. N.; Spitaler, J.; Mühlbacher, M.; Walter, C.; Keckes, J.; Mitterer, C.; Draxl, C. TiO_2(100)/Al_2O_3(0001) interface: A first-principles study supported by experiment. *Phys. Rev. B* **2012**, *86*, No. 205309.
(23) Chen, L.; Li, Y.; Peng, J.; Sun, L.; Li, B.; Wang, Z.; Zhao, S. A comparable study of Fe//MCs (M = Ti, V) interfaces by first-principles method: The chemical bonding, work of adhesion and electronic structures. *J. Phys. Chem. Solids* **2020**, *138*, No. 109292.
(24) Feldbauer, G.; Wolloch, M.; Bedolla, P. O.; Mohn, P.; Redinger, J.; Vernes, A. Adhesion and material transfer between contacting Al and TiN surfaces from first principles. *Phys. Rev. B* **2015**, *91*, No. 165413.
(25) Xie, H.; Chen, Y.; Zhang, T.; Zhao, N.; Shi, C.; He, C.; Liu, E. Adhesion, bonding and mechanical properties of Mo doped diamond/Al (Cu) interfaces: a first principles study. *Appl. Surf. Sci.* **2020**, *527*, No. 146817.
(26) Jarvis, E. A. A.; Carter, E. A. Exploiting Covalency to Enhance Metal-Oxide and Oxide-Oxide Adhesion at Heterogeneous Interfaces. *J. Am. Ceram. Soc.* **2003**, *86*, 373−386.
(27) Spencer, M. J. S.; Snook, I. K.; Yarovsky, I. Effect of Sulfur Impurity on Fe(110) Adhesion: A DFT Study. *J. Phys. Chem. B* **2004**, *108*, 10965−10972.
(28) Lin, Z.; Bristowe, P. D. A density functional study of the effect of hydrogen on the strength of an epitaxial Ag/ZnO interface. *J. Appl. Phys.* **2007**, *102*, No. 103513.
(29) Higuchi, C.; Tanaka, H.; Yoshizawa, K. Molecular understanding of the adhesive interactions between silica surface and epoxy resin: Effects of interfacial water. *J. Comput. Chem.* **2019**, *40*, 164−171.
(30) Kumar, A.; Islam, R.; Pramanik, D.; Saraswat, K. On the limit of defect doping in transition metal oxides. *J. Vac. Sci. Technol., A.* **2019**, *37*, No. 021505.
(31) Smyth, D. M. The effects of dopants on the properties of metal oxides. *Solid State Ionics* **2000**, *129*, 5−12.
(32) Pacchioni, G. Oxygen Vacancy: The Invisible Agent on Oxide Surfaces. *ChemPhysChem* **2003**, *4*, 1041−1047.
(33) Asahi, R.; Morikawa, T.; Irie, H.; Ohwaki, T. Nitrogen-Doped Titanium Dioxide as Visible-Light-Sensitive Photocatalyst: Designs, Developments, and Prospects. *Chem. Rev.* **2014**, *114*, 9824−9852.
(34) Bakar, S. A.; Ribeiro, C. Nitrogen-doped titanium dioxide: An overview of material design and dimensionality effect over modern applications. *J. Photochem. Photobiol., C.* **2016**, *27*, 1−29.

(35) Cong, Y.; Zhang, J.; Chen, F.; Anpo, M. Synthesis and Characterization of Nitrogen-Doped TiO_2 Nanophotocatalyst with High Visible Light Activity. *J. Phys. Chem. C* **2007**, *111*, 6976−6982.
(36) Zhou, Y.; Zhang, Z.; Fang, Z.; Qiu, M.; Ling, L.; Long, J.; Chen, L.; Tong, Y.; Su, W.; Zhang, Y.; Wu, J. C. S.; Basset, J.-M.; Wang, X.; Yu, G. Defect engineering of metal-oxide interface for proximity of photooxidation and photoreduction. *Proc. Natl. Acad. Sci. U.S.A.* **2019**, *116*, 10232.
(37) Zhu, H. X.; Zhou, P. X.; Li, X.; Liu, J.-M. Electronic structures and optical properties of rutile TiO_2 with different point defects from DFT+U calculations. *Phys. Lett. A* **2014**, *378*, 2719−2724.
(38) Tosoni, S.; Chen, H.-Y. T.; Pacchioni, G. A DFT Study of the Reactivity of Anatase TiO_2 and Tetragonal ZrO_2 Stepped Surfaces Compared to the Regular (101) Terraces. *ChemPhysChem* **2015**, *16*, 3642−3651.
(39) Ruiz Puigdollers, A.; Pacchioni, G. Reducibility of ZrO_2/Pt_3Zr and ZrO_2/Pt 2D films compared to bulk zirconia: a DFT+U study of oxygen removal and H_2 adsorption. *Nanoscale* **2017**, *9*, 6866−6876.
(40) Yildirim, H.; Pachter, R. Extrinsic Dopant Effects on Oxygen Vacancy Formation Energies in ZrO_2 with Implication for Memristive Device Performance. *ACS Appl. Electron. Mater.* **2019**, *1*, 467−477.
(41) Luo, H.; Tian, D.; Zeng, C.; Fu, Y.; Wang, H. First-principles study the behavior of oxygen vacancy on the surface of ZrO_2 and $Zr_{0.97}M_{0.03}O_2$. *Comput. Condens. Matter* **2017**, *11*, 1−10.
(42) Yang, J.; Youssef, M.; Yildiz, B. Predicting point defect equilibria across oxide hetero-interfaces: model system of ZrO_2/Cr_2O_3. *Phys. Chem. Chem. Phys.* **2017**, *19*, 3869−3883.
(43) Li, H.; Guo, Y.; Robertson, J. Calculation of TiO_2 Surface and Subsurface Oxygen Vacancy by the Screened Exchange Functional. *J. Phys. Chem. C* **2015**, *119*, 18160−18166.
(44) Magyari-Köpe, B.; Park, S. G.; Lee, H.-D.; Nishi, Y. First principles calculations of oxygen vacancy-ordering effects in resistance change memory materials incorporating binary transition metal oxides. *J. Mater. Sci.* **2012**, *47*, 7498−7514.
(45) Aidhy, D. S.; Zhang, Y.; Weber, W. J. (001) $SrTiO_3$ | (001) MgO Interface and Oxygen-Vacancy Stability from First-Principles Calculations. *ACS Appl. Mater. Interfaces* **2014**, *6*, 15536−15541.
(46) Sun, W.; Zhang, L.; Zhang, Y.; Liu, J.; Wang, H.; Bu, Y. Enhanced works of separation for (0001)ZnO|(111)ZrO_2 interfaces via ion-doping in ZnO: Data-mining and density function theory study. *Comput. Mater. Sci.* **2018**, *142*, 410−416.
(47) Soler, J. M.; Artacho, E.; Gale, J. D.; García, A.; Junquera, J.; Ordejón, P.; Sánchez-Portal, D. The SIESTA Method for Ab Initio Order-N Materials Simulation. *J. Phys.: Condens. Matter* **2002**, *14*, 2745−2779.
(48) Perdew, J. P.; Burke, K.; Ernzerhof, M. Generalized Gradient Approximation Made Simple. *Phys. Rev. Lett.* **1996**, *77*, 3865−3868.
(49) Paulidou, A.; Nix, R. M. Growth and Characterisation of Zirconia Surfaces on Cu(111). *Phys. Chem. Chem. Phys.* **2005**, *7*, 1482−1489.
(50) Gennard, S.; Corà, F.; Catlow, C. R. A. Comparison of the Bulk and Surface Properties of Ceria and Zirconia by Ab Initio Investigations. *J. Phys. Chem. B* **1999**, *103*, 10158−10170.
(51) Balducci, G.; Kašpar, J.; Fornasiero, P.; Graziani, M.; Islam, M. S. Surface and Reduction Energetics of the CeO_2−ZrO_2 Catalysts. *J. Phys. Chem. B* **1998**, *102*, 557−561.
(52) Grau-Crespo, R.; Hernández, N. C.; Sanz, J. F.; de Leeuw, N. H. Theoretical Investigation of the Deposition of Cu, Ag, and Au Atoms on the ZrO2(111) Surface. *J. Phys. Chem. C* **2007**, *111*, 10448−10454.
(53) Wilson, D. J.; Winkler, B.; Juarez-Arellano, E. A.; Friedrich, A.; Knorr, K.; Pickard, C. J.; Milman, V. Virtual Crystal Approximation Study of Nitridosilicates and Oxonitridoaluminosilicates. *J. Phys. Chem. Solids* **2008**, *69*, 1861−1868.
(54) Idé, J.; Cornil, D.; Jacques, A.; Navet, B.; Boulanger, P.; Ventelon, L.; Lazzaroni, R.; Beljonne, D.; Cornil, J. Glass Hardness Modification by Means of Ion Implantation: Electronic Doping versus Surface Composition Effect. *Adv. Theory Simul.* **2019**, *2*, No. 1900039.
(55) Yu, M.; Trinkle, D. R. Accurate and Efficient Algorithm for Bader Charge Integration. *J. Chem. Phys.* **2011**, *134*, No. 064111.
(56) Manz, T. A.; Limas, N. G. Introducing DDEC6 Atomic Population Analysis: Part 1. Charge Partitioning Theory and Methodology. *RSC Adv.* **2016**, *6*, 47771−47801.
(57) Grau-Crespo, R.; Hernández, N. C.; Sanz, J. F.; de Leeuw, N. H. Redox Properties of Gold-Substituted Zirconia Surfaces. *J. Mater. Chem.* **2009**, *19*, 710−717.
(58) Abriata, J. P.; Garcés, J.; Versaci, R. The O-Zr (Oxygen-Zirconium) System. *Bull. Alloy Phase Diagrams* **1986**, *7*, 116−124.
(59) Raza, M.; Cornil, D.; Cornil, J.; Lucas, S.; Snyders, R.; Konstantinidis, S. Oxygen Vacancy Stabilized Zirconia (OVSZ); a Joint Experimental and Theoretical Study. *Scr. Mater.* **2016**, *124*, 26−29.
(60) Kim, B.; Lee, H. Valence State and Ionic Conduction in Mn-Doped MgO Partially Stabilized Zirconia. *J. Am. Ceram. Soc.* **2018**, *101*, 1790−1795.
(61) Drożdż, E. Synthesis, Structural Characterization, Electrical Properties and Chemical Stability of a $(ZrO_2)_{0.97}(Y_2O_3)_{0.03-x}(MgO)_{2x}$ Solid Solution. *RSC Adv.* **2016**, *6*, 84752−84759.
(62) Lee, J.-S.; Lerch, M.; Maier, J. Nitrogen-Doped Zirconia: A Comparison with Cation Stabilized Zirconia. *J. Solid State Chem.* **2006**, *179*, 270−277.
(63) Ricca, C.; Ringuedé, A.; Cassir, M.; Adamo, C.; Labat, F. Revealing the Properties of the Cubic ZrO_2 (111) Surface by Periodic DFT Calculations: Reducibility and Stabilization through Doping with Aliovalent Y_2O_3. *RSC Adv.* **2015**, *5*, 13941−13951.
(64) Zheng, J. X.; Ceder, G.; Maxisch, T.; Chim, W. K.; Choi, W. K. First-Principles Study of Native Point Defects in Hafnia and Zirconia. *Phys. Rev. B* **2007**, *75*, No. 104112.
(65) Chen, H.-Y. T.; Tosoni, S.; Pacchioni, G. A DFT study of the acid−base properties of anatase TiO_2 and tetragonal ZrO_2 by adsorption of CO and CO_2 probe molecules. *Surf. Sci.* **2016**, *652*, 163−171.
(66) Delarmelina, M.; Quesne, M. G.; Catlow, C. R. A. Modelling the bulk properties of ambient pressure polymorphs of zirconia. *Phys. Chem. Chem. Phys.* **2020**, *22*, 6660−6676.
(67) Foster, A. S.; Sulimov, V. B.; Lopez Gejo, F.; Shluger, A. L.; Nieminen, R. M. Modelling of Point Defects in Monoclinic Zirconia. *J. Non-Cryst. Solids* **2002**, *303*, 101−107.
(68) Youssef, M.; Yildiz, B. Intrinsic Point-Defect Equilibria in Tetragonal ZrO_2 Density Functional Theory Analysis with Finite-Temperature Effects. *Phys. Rev. B* **2012**, *86*, No. 144109.
(69) Shen, P. J.; Jiang, S. P.; Ong, K. P.; Ding, W. Z.; Mao, P.-L.; Lu, X. G.; Li, C. H.; Wu, P. Intrinsic Vacancies in Cubic-Zirconia Bulk and Surface. *J. Alloys Compd.* **2010**, *506*, 898−901.
(70) Pan, L.; Ai, M.; Huang, C.; Yin, L.; Liu, X.; Zhang, R.; Wang, S.; Jiang, Z.; Zhang, X.; Zou, J.-J.; Mi, W. Manipulating spin polarization of titanium dioxide for efficient photocatalysis. *Nat. Commun.* **2020**, *11*, No. 418.
(71) Wang, P.; Niu, Y.; Cao, W.; Zhang, Y.; Zhang, M. First-Principles Study of the Effect of Native Defects on Spin Polarization and Exchange Coupling Interaction in Semimetal V_3O_4. *ACS Omega* **2020**, *5*, 9442−9447.

https://dx.doi.org/10.1021/acsami.0c07579
ACS Appl. Mater. Interfaces 2020, 12, 40838−40849